Icarus 242 (2014) 202–210

Contents lists available at ScienceDirect

Icarus

journal homepage: www.elsevier.com/locate/icarus

# Evidence for Middle Amazonian catastrophic flooding and glaciation on Mars

J. Alexis P. Rodríguez [a,b,*], Virginia C. Gulick [a,c], Victor R. Baker [d], Thomas Platz [b,e], Alberto G. Fairén [f], Hideaki Miyamoto [g], Jeffrey S. Kargel [d], James W. Rice [b], Natalie Glines [a]

[a] NASA Ames Research Center, Mail Stop 239-20, Moffett Field, CA 94035, USA
[b] Planetary Science Institute, 1700 East Fort Lowell Road, Suite 106, Tucson, AZ 85719-2395, USA
[c] SETI Institute, 189 Bernardo Ave., Mountain View, CA 94043, USA
[d] Department of Hydrology & Water Resources, University of Arizona, Tucson, AZ 85721, USA
[e] Planetary Sciences and Remote Sensing, Institute of Geological Sciences, Freie Universität Berlin, 12249 Berlin, Germany
[f] Department of Astronomy, Cornell University, 426 Space Sciences Bldg, Ithaca, NY 14853, USA
[g] The University Museum, University of Tokyo, Tokyo 113-0033, Japan

ARTICLE INFO

*Article history:*
Received 13 January 2014
Revised 6 June 2014
Accepted 10 June 2014
Available online 21 July 2014

*Keyword:*
Mars
Surface
Geological processes

ABSTRACT

Early geologic investigations of Mars revealed some of the largest channels in the Solar System (outflow channels), which appear to have mostly developed ~3 byr ago. These channels have been the subject of much scientific inquiry since the 1970s and proposed formative processes included surface erosion by catastrophic floods, glaciers, debris flows and lava flows. Based on the analysis of newly acquired Mars Reconnaissance Orbiter (MRO) Context (CTX, 5.15–5.91 m/pixel) and High Resolution Imaging Science Experiment (HiRISE, 25–50 cm/pixel) image data, we have identified a few locations contained within relatively narrow canyons of the southern circum-Chryse outflow channels that retain well-preserved decameter/hectometer-scale landform assemblages. These terrains include landforms consistent in shape, dimension and overall assemblage to those produced by catastrophic floods, and at one location, to glacial morphologies. Impact crater statistics for four of these surfaces, located within upstream, midstream and downstream outflow channel surfaces, yield an age estimate of ~600 myr. This suggests that the southern circum-Chryse outflow channels were locally resurfaced by some of the most recent catastrophic floods on the planet, and that these floods coexisted within regional glacier environments as recently as during the Middle Amazonian.



## 1. Introduction

The formative processes of the southern circum-Chryse outflow channels (Fig. 1) have been the subject of much scientific inquiry since the 1970s (Baker and Milton, 1974; Carr, 1979) and they are thought to have been excavated on the planet's surface by catastrophic floods (Baker, 1982, 2009a, 2009b), glaciers (Lucchitta, 1982, 2001), $CO_2$-charged debris flows (Hoffman, 2000), $H_2O$-charged debris flows (Nummedal and Prior, 1981), and/or lava flows (Hopper and Leverington, 2014; Leverington, 2011; Schonfeld, 1976). Importantly, the channels appear to mostly be ~3 byr old (Rotto and Tanaka, 1995). The catastrophic flooding hypothesis (Baker, 1982, 2009a, 2009b) is particularly compelling in that many of the morphological features in the outflow channels, which were largely identified using Viking orbiter image mosaics (~50–230 m/pixel), bear a striking resemblance in shape to (but are significantly larger than) bedforms produced as a result of terrestrial catastrophic floods in the Channeled Scablands in Washington State during the Pleistocene (Baker and Milton, 1974). Furthermore, many of these outflow channels extend from extensive zones of upper crustal collapse, known as chaotic terrains, which were likely produced as a result of rapid aquifer evacuation (Carr, 1979). In addition, catastrophic flood discharges from vast paleo-lakes within central (Lucchitta et al., 1994) and eastern (Warner et al., 2013b) Valles Marineris might also have inundated Simud and Tiu Valles. The lower floors of these outflow channels are connected to Valles Marineris via Capri and Eos chasmata (Fig. 1b).

* Corresponding author at: NASA Ames Research Center, Mail Stop 239-20, Moffett Field, CA 94035, USA.
*E-mail address:* Alexis.Rodriguez@NASA.gov (J.A.P. Rodríguez).

http://dx.doi.org/10.1016/j.icarus.2014.06.008
0019-1035/

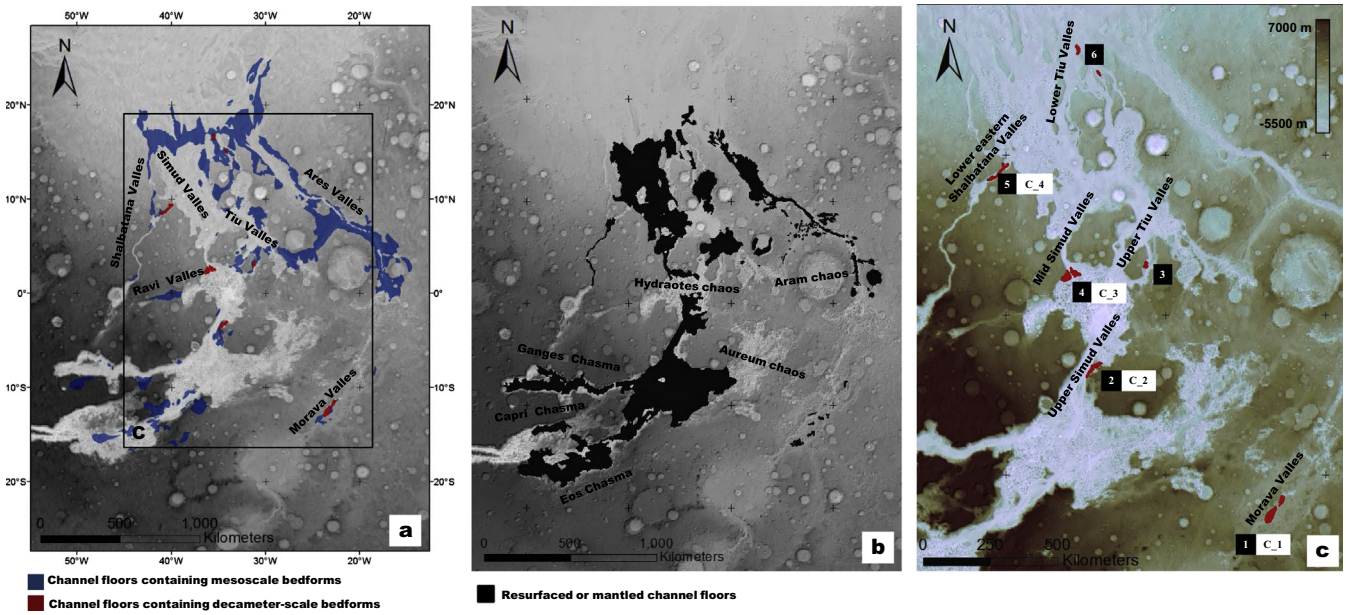


**Fig. 1.** (a) Zonal distribution map showing outflow channel floors that exhibit especially well-preserved mesoscale (several hundred meters to kilometers) and decameter/hectometer-scale bedforms in southern circum-Chryse. (b) Map showing the distribution of outflow channel floors that are extensively mantled or resurfaced. (c) Close-up view on the region that contains the channel surfaces with the decameter/hectometer-scale bedforms, which are labeled 1–6. The maps were produced using Environmental Systems Research Institute's (ESRI) ArcGIS.

## 2. Remote sensing data analyses and interpretative synthesis

Using MRO CTX and HiRISE image data in combination with Mars Odyssey Thermal Emission Imaging System (THEMIS, ~512 pixels per degree) day and night Infrared (IR) mosaics and Mars Orbiter Laser Altimeter (MOLA, ~460 m/pixel horizontal and ~1 m vertical resolution) surface topography, we have produced a zonal distribution map of terrains within the southern circum-Chryse outflow channels that exhibit especially well-preserved mesoscale (several hundred meters to kilometers) and smaller (decameter/hectometer-scale) bedforms (Fig. 1a and c). In addition, we have also mapped the zones within these outflow channels where the floors appear mostly mantled or resurfaced (Fig. 1b).

Although the mapped outflow channels containing mesoscale bedforms appear more extensive and better integrated within NE southern circum-Chryse (Fig. 1a), the identified decameter/hectometer-scale bedforms are located mostly to the SW of the region, where they are sparsely distributed in Shalbatana, Simud/Tiu, and Morava Valles (Fig. 1a and c). These surfaces are likely more susceptible to regional resurfacing and mantling processes due to their modest relief (~10s of meters). Detectability of these smaller set of landforms within the southern circum-Chryse might increase with further HiRISE coverage of outflow channel floors (Fig. 1a).

In this paper, we propose probable formational mechanisms and provide age estimates for decameter/hectometer-scale bedform assemblages contained within the mapped floors (Fig. 2, Table 1, Annex), which include upstream, midstream, and downstream portions of the southern circum-Chryse outflow channels. In THEMIS night IR images, the upstream and midstream surfaces appear bright (e.g., Figs. 3a, 5a, 6a and c), indicating that they mostly likely consist of bedrock and/or rocky exposures (Christensen et al., 2003).

The investigated upstream terrain occurs within Morava Valles, a high elevation outflow channel situated at ~10°S (location 1 in Fig. 1c). An investigated zone of this outflow channel's lower reaches (Fig. 3b) reveals a possible lateral moraine and adjacent kettle holes (Fig. 4a–e, Table 2). In contrast, a zone within its upper reaches (Fig. 3c) reveals possible drumlins, rogen moraines, longitudinal grooves and ridges as well a deeply entrenched furrows (Figs. 3c and 4f–i, Table 2). These bedform assemblages are oriented in a northeasterly direction following the channel's downstream trend, which would be consistent with resurfacing by wet-based glacial flow (hollow white arrows in Fig. 3). Terrestrial lateral moraines and kettle holes occur in association along the margins of glaciers' downstream portions, which tend to be dominated by outwash sedimentation (Bennett and Glasser, 2009). On the other hand, drumlins, rogen moraines and pronounced scouring are thought to develop by glacial ice acting on underlying bedrock and sediments (Bennett and Glasser, 2009), or by subglacial catastrophic flooding (Bennett and Glasser, 2009). Consequently, we propose that the Morava Valles included a continuous glacier that stretched at least 50 km in length (Fig. 3a).

The investigated midstream locations include three subequatorial surfaces (locations 2–4 in Fig. 1c), which form rocky pockets of materials within otherwise extensively mantled or resurfaced low elevation outflow channels (Fig. 1b). The identified bedforms within these surfaces (Figs. 5 and 6) are analogous in shape, scale as well as overall assemblage to landforms within the Channeled Scablands located in eastern Washington (Fig. 7). These terrestrial channels formed in columnar jointed flood basalts by catastrophic flood erosion due to giant outbursts from a Pleistocene ice-dammed lake, Glacial Lake Missoula (Baker, 2009a). Columnar jointing, or other similar fracture-riven rock structures, are thought to be critical to Scabland-type catastrophic flood erosion (Baker, 2009a, 2009b). In particular, upper Simud Valles (location 2 in Figs. 1c and 5a–h), retains an extensive record of Channeled Scablands analogous landforms. These include ridges and polygonal fractures that resemble exhumed dikes and fractured basalt (Fig. 5c and d), as well as exceptionally well-preserved bedforms, including, analogous streamlined mesas (Fig. 5b), bouldery fluvial dunes, inner entrenched channels, longitudinal grooves and ridges, and butte-and-basin morphologies (Fig. 5e–h, Table 2). Although only covered by CTX, the midstream section of Simud Valles (location 4 in Figs. 1c and 6a) contains a landform that is analogous to a cataract (Fig. 6b, Table 2). In addition, upper Tiu Valles (location 3

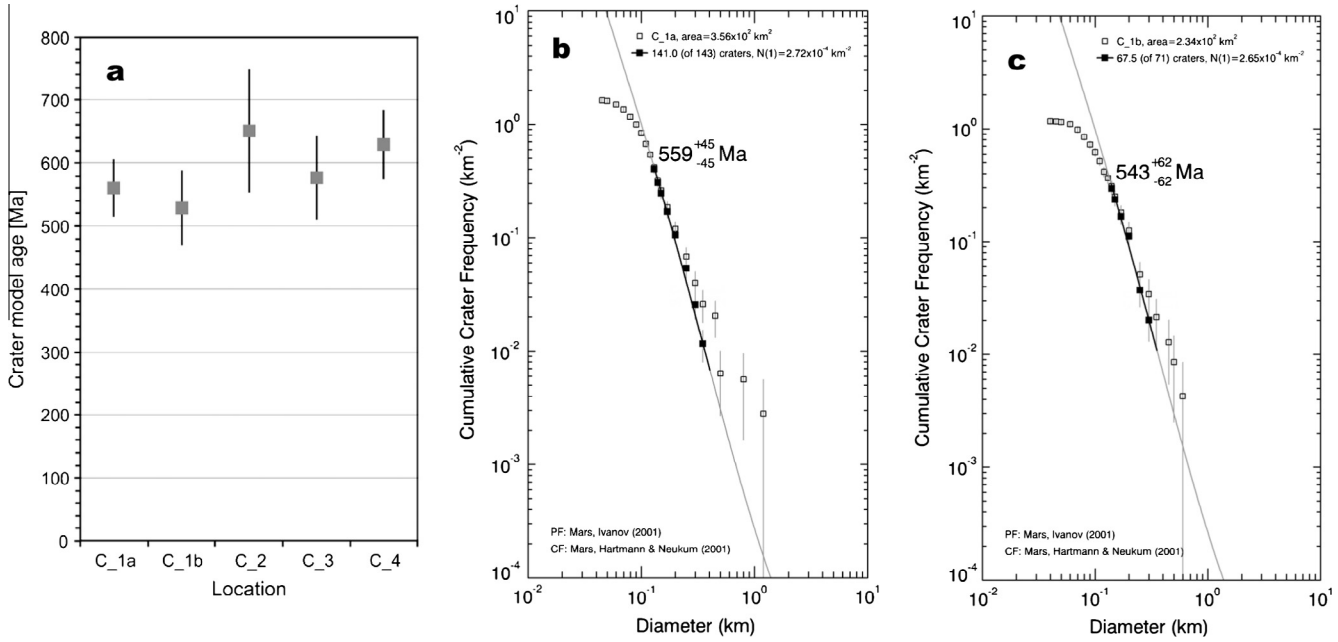


**Fig. 2.** (a) Crater model ages for locations C_1 to C_4 in panel c of Fig. 1c. Other locations do not possess enough CTX coverage to derive significant statistics from impact crater counts. All surfaces show best-fit formation ages of ~526–650 Ma. Panels b and c show the cumulative plots for surfaces C_1a and C_1b. Crater statistics were measured and analyzed with *CraterTools* (Kneissl et al., 2011) and *Craterstats* (Michael and Neukum, 2010; Michael et al., 2012) following the description presented in Platz et al. (2013). The chronology (Hartmann and Neukum, 2001) and production (Ivanov, 2001) functions were used to derive crater model ages. Note filled squares represent bins to which a resurfacing correction was applied to the cumulative plot (Michael and Neukum, 2010). See Annex for details regarding the reverse-cumulative and differential crater size–frequency distributions along with context maps and documentation of mapped impact crater populations.

**Table 1**
Absolute model ages for four locations. Locations are documented in Fig. 1 and in the Annex. Detailed crater statistics are provided in the Annex.

| Location | Coordinates[a] (°) | | Area (km$^2$) | Age (Ma)[b] | | | | | $N_{cum}$ (1 km) /10$^6$ km$^2$ of fitted isochron | |
|---|---|---|---|---|---|---|---|---|---|---|
| | Latitude | Longitude west | | Best fit | Error + | Error − | Max. fit | Min. fit | | Error +/− |
| C_1a | −12.21 | −23.34 | 356.0 | 559 | 45 | 45 | 604 | 514 | 2.72E−04 | 2.19E−05 |
| | −12.55 | −23.33 | | | | | | | | |
| C_1b | −11.54 | −22.72 | 234.3 | 543 | 62 | 62 | 605 | 481 | 2.65E−04 | 3.01E−05 |
| C_2 | −3.19 | −34.44 | 391.5 | 650 | 97 | 97 | 747 | 553 | 3.17E−04 | 4.73E−05 |
| C_3 | 2.36 | −36.17 | 827.6 | 576 | 66 | 66 | 642 | 510 | 2.81E−04 | 3.23E−05 |
| | 2.64 | −35.67 | | | | | | | | |
| C_4 | 9.03 | −40.3 | 270.3 | 628 | 55 | 55 | 683 | 573 | 3.06E−04 | 2.70E−05 |

[a] Centre coordinates of counting area; multiple coordinates mean multiple subareas.
[b] Crater size–frequency distribution absolute model ages are derived using the production function of Ivanov (2001) and the Neukum chronology function of Hartmann and Neukum (2001).

in Figs. 1c and 6c), is marked by inner channel entrenchment (arrow 1 in Fig. 6d, Table 2), longitudinal ridges (arrow 2 in Fig. 6d, Table 2), and possible butte-and-basin topography (arrow 3 in Fig. 6d, Table 2).

Individual landforms might also be explained by other flow processes such as with $CO_2$ (Hoffman, 2000) or lava as medium (Hopper and Leverington, 2014; Leverington, 2011). Nevertheless, the entire suite of observed landforms and their analogous relationship to those formed by cataclysmic flooding, provide a powerful indication that this was the formative process (Baker, 1982, 2012). In particular, the spatial association of butte-and-basin topography, longitudinal grooves, cataracts and inner channels (Fig. 7) require macroturbulent flow eroding on fractured bedrock (Baker, 1979, 1982), which would only be generated by large-scale, low-viscosity flows such as catastrophic floods. We note that this morphologic assemblage could have also been generated by fast-flowing subglacial meltwater, as it is likely the case within a 500-km-long system of bedrock channels known as the Labyrinth located in the western Dry Valleys of Antarctica (Lewis et al., 2006). Thus, we propose that these bedform assemblages indicate resurfacing by catastrophic floods or fast moving subglacial meltwater. In addition, the orientations of the investigated bedforms are consistent with those that would have resulted by downstream flow propagation (hollow white arrows in Figs. 5b and 6a and c).

The investigated downstream surfaces, situated at ~10°S (locations 5 and 6 in Fig. 1c), include a location in lower eastern Shalbatana Valles (Fig. 8a) and another in lower Tiu Valles (Fig. 8e). These channel surfaces appear darker in THEMIS night IR imagery (Fig. 8a and e) than the investigated upstream sites (Figs. 5a and 6a and c), indicating that their surfaces must contain a relatively higher proportion of fine grained sediments (Christensen et al., 2003). These channel surfaces exhibit systems of transverse ridges (Fig. 8c and f, Table 2). At the Shalbatana Valles site these are morphologically analogous to terrestrial fluvial dunes (Fig. 8d). However, at the Tiu Valles site these appear to be morphologically analogous to transverse ribs (also known as antidunes) (Fig. 8g and h). These landforms are modified by the impact crater populations within the floors (Fig. 8c and f), indicating that their ages must be those of floor emplacement. At the Shalbatana Valles site there is an impact crater, ~750 m in diameter, which exposes the upper strata

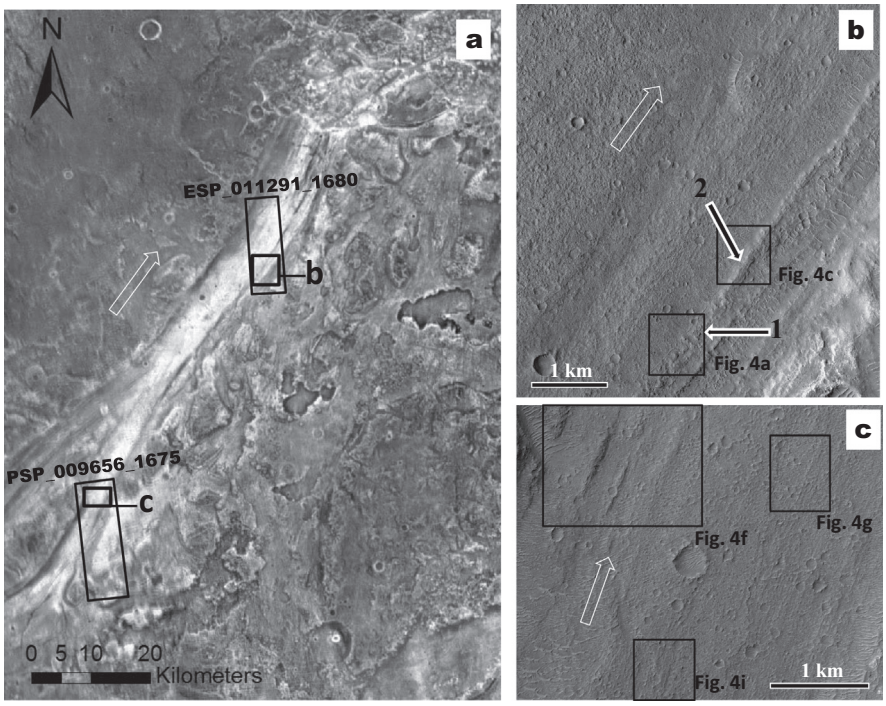


**Fig. 3.** (a) THEMIS night IR view of Morava Valles (location 1 in Fig. 1c) showing the portions of examined channel surfaces within HiRISE images ESP_011291_1680 and PSP_009656_1675 (panels b and c). (b) View of northern Morava Valles providing context and locations for panels a and c in Fig. 4. Part of HiRISE image ESP_011291_1680 (25 cm/pixel) centered at 11°47′S, 22°47′W. (c) View of southern Morava Valles providing context and locations for panels f, g and i in Fig. 4. Part of HiRISE image PSP_009656_1675 (25 cm/pixel) centered at 12°27′S, 23°17′W.

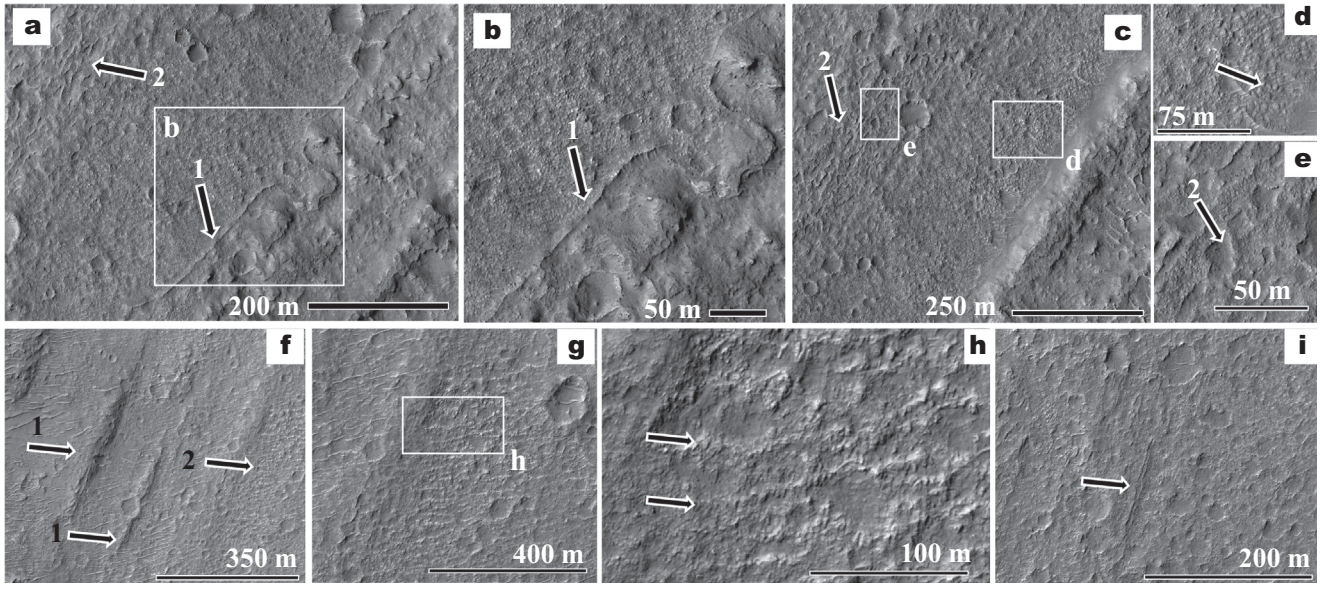


**Fig. 4.** (a and b) Curvilinear ridge with well-defined crest interpreted as a lateral moraine (arrows 1) that marks the contact between a bouldery field and the margin of a highly degraded section of an older longitudinal ridge (arrow 1 in Fig. 3b). Approximately 1 km downstream a better preserved section of the longitudinal ridge (arrow 2 in Fig. 3b) is flanked by a talus that contains boulders as large as ~5 m across (c and d). The bouldery field enclosed by the proposed lateral moraine exhibits clusters of elongate depressions interpreted as a kettle holes (arrows labeled 2 in a, c and e). (f) Elongate and narrow scoured promontories interpreted as drumlins (arrows 1) occur in association with ridges (arrow 2) oriented roughly orthogonal to the promontories lengths. These ridges, which we interpret as rogen moraines, form extensive fields (g) and appear to consist of large bouldery deposits (h). (i) Elongate trench mark along the channel.

forming the floor materials (arrow 1, Fig. 8b and c). These materials appear bright in THEMIS night IR imagery, indicating that the floor deposits likely consist of coarse sediments mantled by finer-grained deposits. Fluvial dunes formed by catastrophic flooding on Earth often contain many coarse grains up to boulders (Carling, 1996; Komatsu et al., 2009). We also note that materials that comprise the possible fluvial dunes do not exhibit evidence for aeolian remobilization into bedforms or streaks as would be expected if they consisted of fine-grained sediments. In fact, regional aeolian mantles appear significantly darker than the floors marked by the possible fluvial dunes (arrow 2 in Fig. 8a–c).

Transverse ribs (antidunes) consist of trains of regularly spaced gravel symmetrical ridges that are mostly oriented oblique to the main direction of flow (Fig. 8g and h) (Carling, 1999). They are

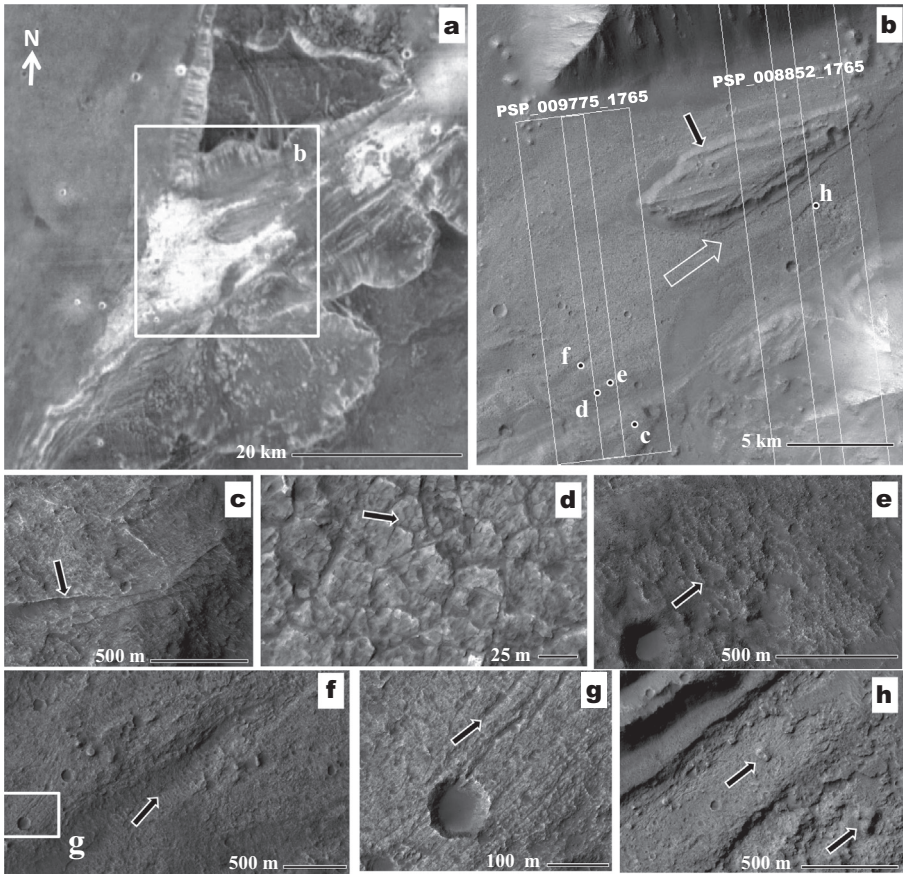


**Fig. 5.** Midstream reaches of the southern circum-Chryse outflow channels. (a) THEMIS night IR view of bright surfaces indicative of bedrock/rocky surfaces in upper Simud Valles (location 2 in Fig. 1c). (b) Part of CTX mosaic (5.15–5.91 m/pixel) showing the locations panels c–f and h) within HiRISE images PSP_009775_1765 and PSP_008852_1765 (both 25 cm/pixel). The hollow white arrow indicates inferred flow direction. (c) Surface exposure showing possible dikes (black arrow). Part of HiRISE image centered at 3°22′S, 34°32′W. (d) Surface exposure showing possible columnar joints or other similar fracture-riven rock structures. Arrow points to the margins of a possible column's head that is 3.5 m across, which is comparable to the dimension of terrestrial counterparts. Part of HiRISE image centered at 3°21′S, 34°34′W. (e) Surface exposure showing possible bouldery fluvial dunes. Part of HiRISE image centered at 3°21′S, 34°34′W. (f) Entrenched inner channel. Part of HiRISE image centered at 3°20′S, 34°35′W. (g) Longitudinal grooves and ridges [close-up view on panel f]. (h) Butte-and-basin morphologies. Part of HiRISE image centered at 3°12′S, 34°24′W.

generally straight and continuous over long distances, but locally show bifurcations (Carling, 1999). These bedforms develop in transitional and supercritical flows and their average wave length corresponds to the typical spacing between standing waves in the flows (Carling and Shvidchenko, 2002; Koster, 1978). Koster (1978) developed equations that permit the estimation of the mean velocity, mean depth, and Froude number from transverse rib data, making the investigation of these features particularly useful for paleo-hydraulic determinations (Carling et al., 2009b; Rice et al., 2002).

Based on morphometric analysis of selected Mars Orbiter Camera (MOC) images, possible transverse ribs have been identified on the floors of Ares and Tiu Valles in southern circum-Chryse (average wave length is 59 m, (Rice, 2000)) and Athabasca Valles (average wave length is 53.6 m, (Rice et al., 2002)). Those shown in Fig. 8f are located within a relatively narrow canyon (~8 km wide) in lower Tiu Valles. Funneling of the floods along the canyon would have increased the water's depth, generating more distantly spaced transverse ribs than in other wider sections of the outflow channel investigated by Rice (2000). Indeed, we find that the bedforms exhibit an average wave length of ~190 m, which would have been generated in floods with an average depth ~30 m (Koster, 1978). The wavelength of the possible transverse ribs in lower Tiu Valles closely approximates those of transverse ribs recently discovered in British Columbia Canada. These terrestrial transverse ribs have wavelengths between ~100 and ~230 m (Johnsen and Brennand, 2004), and would have developed in water depths ranging from ~16 to ~36 m (Carling et al., 2009b). As expected, the proposed fluvial dunes and transverse ribs are oriented perpendicular to the lengths of the outflow channel canyons within which they occur, and are therefore consistent with the overall expected flow directions (hollow white arrows in Fig. 8c and f).

The investigated surfaces containing channeled-scabland-like bedforms occur within relatively narrow canyon sections of the southern circum-Chryse outflow channels that are neither extensively mantled nor resurfaced (Fig. 1a and b). The overall higher degree of constriction within the midstream outflow channel reaches would have resulted in higher flow velocities and the development of channel floors characterized by predominantly erosional morphologies (Rodriguez et al., 2006). In contrast, the dominance of depositional morphologies within the downstream reaches is consistent with overall broader and less constricted channel portions in these regions (Rodriguez et al., 2006).

Our impact crater statistic studies suggest that the mapped channel floor materials containing the decameter/hectometer-scale bedforms formed ~600 Ma (late Middle Amazonian) (Fig. 2, Table 1, Annex). In contrast, older channel floors containing kilometer-scale bedforms (Fig. 1a) are considered to have primarily occurred during the Late Hesperian (Rotto and Tanaka, 1995) but their formational history might have spanned episodically from Late Noachian (Warner et al., 2013a) until Early Amazonian

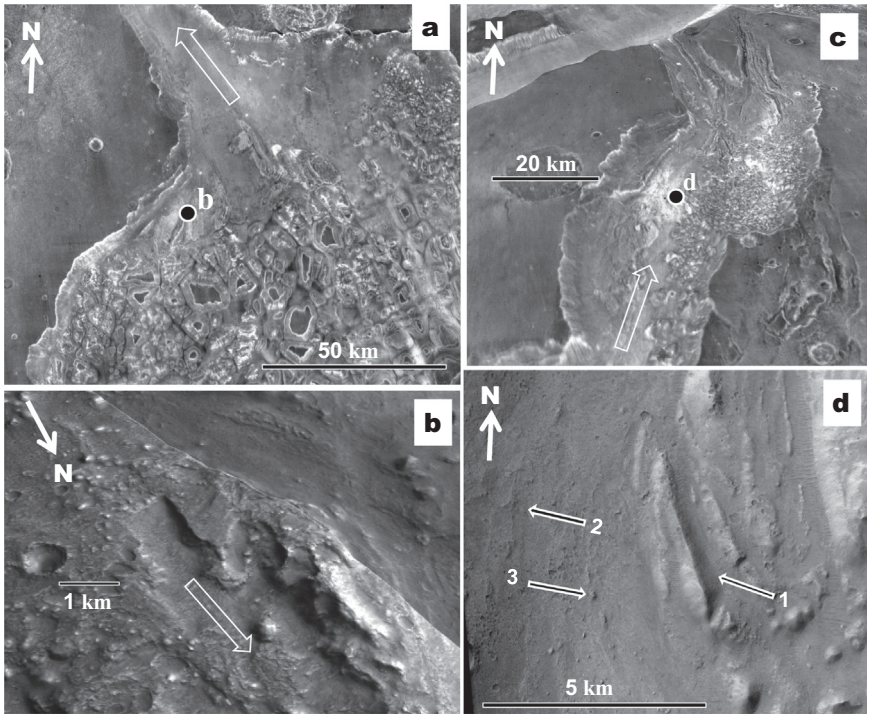


**Fig. 6.** Midstream reaches of the southern circum-Chryse outflow channels. (a) THEMIS night IR view of mid Simud Valles (location 4 in Fig. 1c). (b) Close-up view on location 4 shows cataracts. Part of CTX mosaic (5.15–5.91 m/pixel) centered at 2°21′N, 36°10′W. (c) THEMIS night IR view of upper Timud Valles (location 3 in Fig. 1c). (d) Close-up view on location 3 shows inner channel entrenchment (arrow 1), longitudinal ridges (arrow 2) and possible butte-and-basin morphologies (arrow 3). Part of CTX mosaic (5.15–5.91 m/pixel) centered at 3°8′N, 31°9′W.

(Warner et al., 2013b). The inferred episodes of catastrophic flooding and glacial erosion represent the youngest stages of outflow channel activity in southern circum-Chryse thus far identified.

## 3. Discussion and implications

Our investigation reveals closer analogs to the Channeled Scabland landforms than had been inferred from the lower resolution data. However, the discharge magnitude of floods that formed these surfaces might differ from those that formed the Channeled Scablands because fully turbulent flow discharges depend largely on a resistance coefficient, which is difficult to estimate even on Earth. Furthermore, uncertainties in the estimated flow depths could have caused overestimation of flow rates by a factor of twenty-five (Wilson et al., 2004). However, the capacity for bedrock erosion is much less sensitive to these uncertainties. Turbulent flows will begin to erode the channel bed (basalt bedrock in this case) when the bed shear stress exceeds a threshold that depends on its material strength. Therefore, the erosional features documented in this work have significant implications for understanding the nature of the flows forming the outflow channels. Because bed shear stress is directly proportional to both flow depth and gravity, the existence of similar-sized erosion features on Mars, with its reduced gravity relative to Earth, implies that the flow depths associated with the Mars erosion were about three times greater than those associated with the similar erosion forms on Earth.

On Earth, channels excavated by catastrophic floods are typically the result of large-scale discharges from upstream ice-dammed lakes or subglacial eruptions (Baker, 2009a, 2009b; Grosswald, 1999; Montgomery et al., 1997; Teller, 2004), pointing to the possibility that the proposed stage in catastrophic flooding on Mars resulted in a similar manner.

Our investigation points to Middle Amazonian (~600 Ma) glaciation that was linked to coeval episodes of downstream catastrophic floods, perhaps discharged as jökullaups, occurring within the southern circum-Chryse outflow channels. In the midstream sections of the outflow channels the catastrophic floods might have been mostly ice-covered (Table 2). However, the occurrence of transverse ribs and fluvial dunes in their downstream sections (Fig. 8a and e) indicates that in these regions the floods mostly occurred subaerially. This is because antidunes and fluvial dunes form underneath standing surface waves (Carling et al., 2009a) (Table 2).

In addition, the presence of preserved antidunes and fluvial dunes usually indicates rapid recession of flood flow (Alexander and Fielding, 1997). In this sense, the documented stage of flooding in southern circum-Chryse likely experienced an abrupt draw down, indicating that the catastrophic floods were not followed by episodes of non-catastrophic fluvial dissection as has been reported in some of the older outflow channels (Williams and Malin, 2004).

Our crater count statistics (Fig. 2, Table 1, Annex) indicate that the proposed glacial and periglacial environments in southern circum-Chryse developed during the Middle Amazonian, a period during which Mars seems to have experienced episodic, relatively short-duration climatic warming as inferred, for example, from the discovery of extensive resurfacing of water–ice rich northern plains materials (Skinner et al., 2012). Climate change as a trigger for outflow channel activity is an interesting and novel possibility, which advocates a reverse relationship to that proposed to have occurred during the much earlier stages of Late Hesperian outflow channel activity, in which the floods are thought to have caused global climate change (Baker et al., 1991; Gulick et al., 1997) as well as to the development of regional glacial and periglacial environments (Gulick et al., 1997; Pacifici et al., 2009).

The Late Hesperian southern circum-Chryse outflow channels appear to have mostly formed as vast volumes of groundwater erupted at the surface, a process that led to extensive collapse and chaotic terrain formation (Baker et al., 1992; Carr, 1979;

**Table 2**
Compatibility table linking identified morphologic features at the investigated locations (Fig. 1) to formational processes on Earth. The favored landform interpretation is based on assemblage completeness (highlighted in bold).

| | Morphological features | Terrestrial formational process | | | | | Favored landform interpretation |
|---|---|---|---|---|---|---|---|
| | | Wind | Mud flow | Glacier | Lava | Catastrophic floods | |
| *Upstream location* | | | | | | | |
| Location 1 | Marginal bouldery levees | – | X | **X** | – | X | Lateral moraine |
| (Figs. 3 | Depressions within bouldery deposits | – | – | **X** | – | – | Kettle holes |
| and 4) | Streamlined ridges developed in resistant materials | – | X | **X** | – | X | Spindle-shaped Drumlins |
| | Ribbed bouldery surfaces transverse to the channel's length | – | – | **X** | – | X | Rogen moraines |
| | Deep furrows | – | X | **X** | – | X | Erosion produced by ice or rocks being dragged along the bedrock |
| | Longitudinal grooves and ridges | – | X | **X** | – | X | Glacial basal scour marks |
| *Midstream locations* | | | | | | | |
| Location 2 | Teardrop-shaped promontories | – | X | X | – | **X** | Mesas streamlined by floods |
| (Fig. 5) | Inner channel development within bedrock | – | – | X | – | **X** | Zones of differential erosion by floods |
| | Ribbed bouldery surfaces transverse to the channel's length | – | – | X | – | **X** | Fluvial dunes |
| | Longitudinal grooves and ridges | – | X | X | – | **X** | Scour marks produced by longitudinal vortices |
| | Butte-and-basin topography | – | – | – | – | **X** | Bedrock plucking by turbulent floods |
| Location 3 | Teardrop-shaped promontories | – | X | X | – | **X** | Mesas streamlined by floods |
| (Fig. 6a | Inner channel development within bedrock | – | – | X | – | **X** | Zones of differential erosion by floods |
| and b) | Longitudinal grooves and ridges | – | X | X | – | **X** | Scour marks produced by longitudinal vortices |
| | Butte-and-basin topography | – | – | – | – | **X** | Bedrock plucking by turbulent floods |
| Location 4 | Teardrop-shaped promontories | – | X | X | – | **X** | Mesas streamlined by turbulent flows |
| (Fig. 6c | Inner channel development within bedrock | – | – | X | – | **X** | Zones of differential erosion by turbulent flows |
| and d) | Longitudinal grooves and ridges | – | X | X | – | **X** | Scour marks produced by longitudinal vortices |
| | Butte-and-basin topography | – | – | – | – | **X** | Bedrock plucking by turbulent flows which could have occurred subglacially or subaerially |
| | Cataract-like scarp | – | – | – | – | **X** | Bedrock undercutting by turbulent flows |
| *Downstream locations* | | | | | | | |
| Location 5 | Widespread ripples oriented perpendicular to | – | – | – | – | **X** | Fluvial dunes |
| (Fig. 8a-c) | the lengths of the outflow channel canyons | | | | | | |
| Location 6 | Widespread ripples oriented perpendicular to | – | – | – | – | **X** | Antidunes |
| (Fig. 8e | the lengths of the outflow channel canyons | | | | | | |
| and f) | | | | | | | |

*Note:* Fluvial dunes and transverse ribs develop and below standing waves, thus we have favored a sub-aerial catastrophic flooding origin at locations 2, 5 and 6. However, the butte-and-basin topography and cataract-like scarps in locations 3 and 4 could have also developed by subglacial catastrophic flooding.

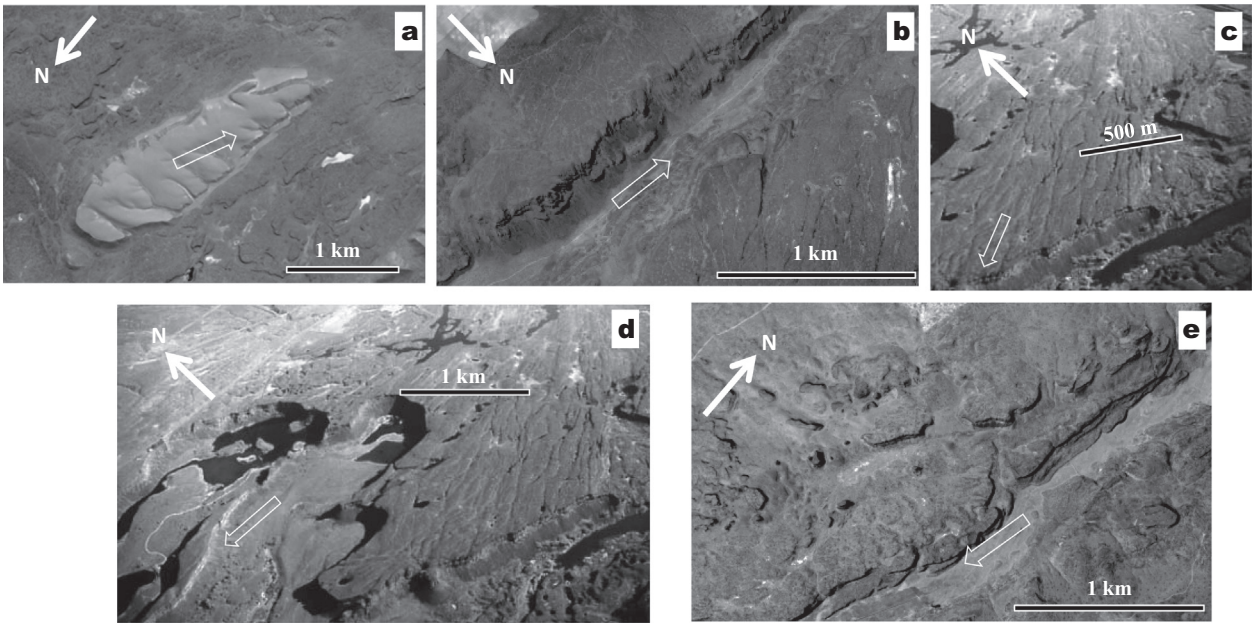


**Fig. 7.** Channeled Scablands landforms. (a) Streamlined mesa. Part of SPOT 5 image mosaic (5 m/pixel) centered at 47°5′N and 118°5′W. (b) Entrenched inner channel. Part of SPOT 5 image mosaic (5 m/pixel) centered at 47°32′N, 119°24′W. (c) Longitudinal grooves and ridges. Part of aerial view centered at 47°35′N, 119°20′W. (d) Cataracts. Part of aerial view centered at 47°35′N, 119°21′W. (e) Butte-and-basin morphologies. Part of SPOT 5 image mosaic (5 m/pixel) centered at 47°21′N, 118°45′W.

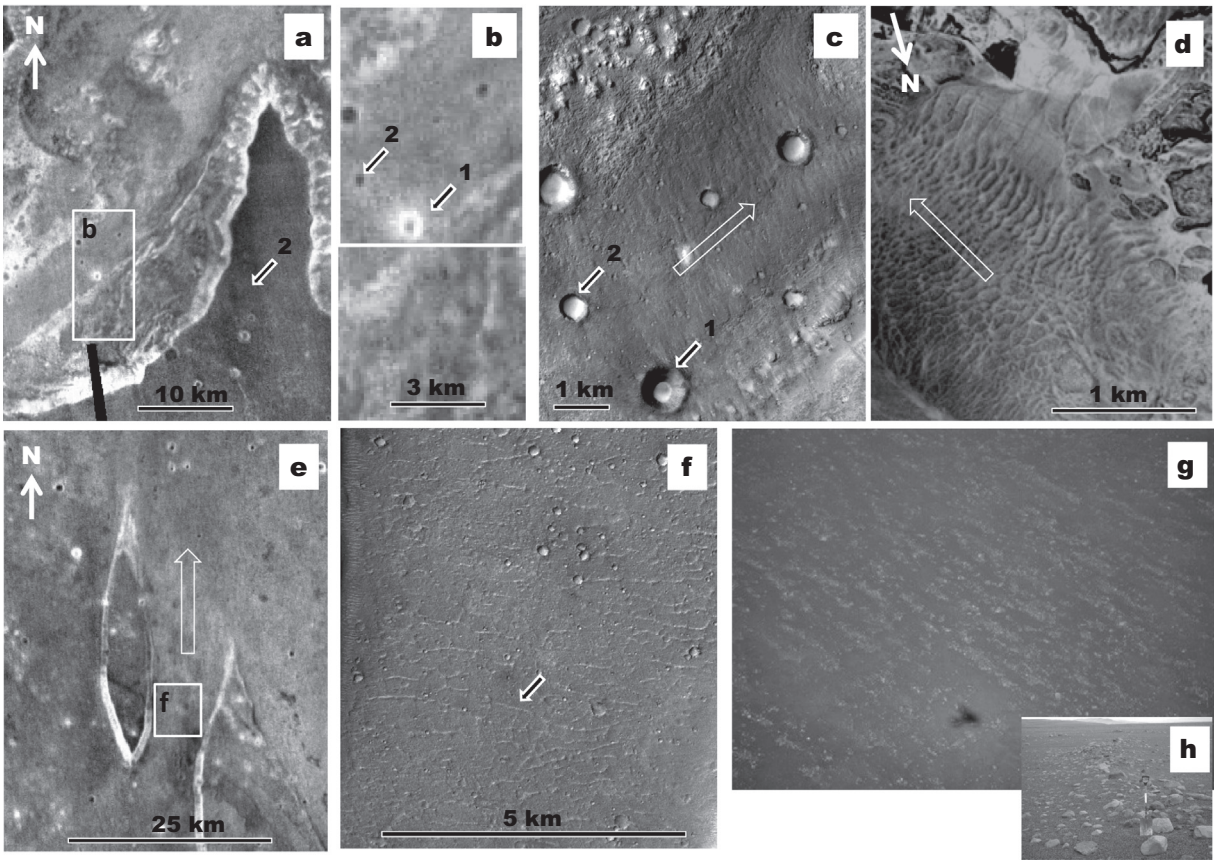


**Fig. 8.** Downstream reaches of the southern circum-Chryse outflow channels. The hollow white arrows indicate inferred flow direction. (a) THEMIS night IR view of lower eastern Shalbatana Valles [location 5 in Fig. 1c]. (b) Close-up view on panel a shows a bright and a dark zones (arrows 1 and 2), which respectively correspond to impact crater wall materials and crater interior aeolian sediments (arrows 1 and 2 in panel c). (c) Close-up view reveals possible fluvial dunes. Part of CTX mosaic (5.15–5.91 m/pixel) centered at 9°20′N, 39°58′W. (d) Fluvial dunes in Channeled Scablands. Part of SPOT 5 image mosaic (5 m/pixel) centered 47°25′N, 118°59′W. (e) THEMIS night IR view of lower Tiu Valles [location 6 in Fig. 1c]. (f) Possible transverse ribs. Part of CTX mosaic (5.15–5.91 m/pixel) centered at 16°28′N, 35°29′W. (g) High-angle oblique aerial view of regularly spaced gravel ridges at Modrudalur in Iceland that have been interpreted to be transverse ribs or antidunes. The features have average wavelengths of 27 m, heights of 0.8 m and breadths of 14 m. Shadow is of a light aircraft. (h) View along a ridge shown in panel g. Largest boulders are 1.8 m long. Spade for scale is 1 m in length. (Photographs courtesy of Dr. Jim Rice and caption information from Rice et al. (2002).)

Meresse et al., 2008; Rodriguez et al., 2005; Rotto and Tanaka, 1995). Elsewhere on Mars, sites of possible Late Amazonian catastrophic floods include Marte Vallis (70 Ma), Grjota Valles (10–40 Ma) and Athabasca Valles (4 Ma) (Burr et al., 2002). These also appear to have had groundwater sources and their generation has been attributed to a combination of tectonic and magmatic processes (Burr et al., 2002).

Here, we propose that the Middle Amazonian climate warming led to the melting and flow of ancient relict ice contained within the outflow channel floors. The ice deposits might comprise remnants of frozen Late Hesperian floods (Pacifici et al., 2009). In addition, melting of the remnant of a Late Noachian ice sheet within Valles Marineris (Gourronc et al., 2014) could have also contributed to our proposed stage of outflow channel activity.

Even more recent episodes of climate change also appear to have occurred during the Late Amazonian as inferred on the basis of evidence for glaciation at tropical latitudes during the past ~2 Ma, which likely resulted from obliquity variations (Head et al., 2005). Thus, it appears that the Amazonian period might have been characterized by extremely cold and dry long periods punctuated by short-duration climatic warming that allowed for glacier formation, which at least during the Middle Amazonian, appear to have occurred in combination with significant meltwater production, pointing to a more active Amazonian surface hydrosphere for Mars than previously considered.

## Acknowledgments

Funding provided by NASA's NPP program to J. Alexis P. Rodriguez and by MRO HiRISE Co-Investigator funds to V.C. Gulick. T. Platz was supported by a DFG grant (PL613/2-1) and the Helmholtz association through the research alliance "Planetary Evolution and Life". HiRISE images were analyzed using HiView developed by the Lunar and Planetary Laboratory at the University of Arizona.The participation of Hideaki Miyamoto was supported by grant KAKENHI 23340126.

## Appendix A. Supplementary material

Supplementary data associated with this article can be found, in the online version, at http://dx.doi.org/10.1016/j.icarus.2014.06.008.

## References

Alexander, J., Fielding, C., 1997. Gravel antidunes in the tropical Burdekin River, Queensland, Australia. Sedimentology 44, 327–337.
Baker, V.R., 1979. Erosional processes in channelized water flows on Mars. J. Geophys. Res. 84, 7985–7993.
Baker, V.R., 1982. The Channels of Mars. University of Texas Press, Austin, Texas.
Baker, V.R., 2009a. The Channeled Scabland—A retrospective. Annu. Rev. Earth Planet. Sci. 37, 6.1–6.19.

Baker, V.R., 2009b. Channeled Scabland Morphology. Cambridge University Press, Cambridge.
Baker, V.R., 2012. Terrestrial analogs, planetary geology, and the nature of geological reasoning. Planet. Space Sci.. http://dx.doi.org/10.1016/j.pss.2012.10.008.
Baker, V.R., Milton, D.J., 1974. Erosion by catastrophic floods on Mars and Earth. Icarus 23, 27–41.
Baker, V.R., Strom, R.G., Gulick, V.C., Kargel, J.S., Komatsu, G., Kale, V.S., 1991. Ancient oceans, ice sheets and the hydrological cycle on Mars. Nature 352, 589–594.
Baker, V.R., Carr, M.H., Gulick, V.C., Williams, C.R., Marley, M.S., 1992. Channels and valley networks. Mars, 493–522.
Bennett, M.M., Glasser, N.F., 2009. Glacial Geology: Ice Sheets and Landforms, second ed. Wiley and Blackwell.
Burr, D.M., Grier, J.A., McEwen, A.S., Keszthelyi, L.P., 2002. Repeated aqueous flooding from the Cerberus Fossae: Evidence for very recently extant, deep groundwater on Mars. Icarus 159, 53–73.
Carling, P.A., 1996. Morphology, sedimentology and palaeohydraulic significance of large gravel dunes, Altai Mountains, Siberia. Sedimentology 43, 647–664.
Carling, P.A., 1999. Subaqueous gravel dunes. J. Sediment. Res. 69, 534–545.
Carling, P.A., Shvidchenko, A.B., 2002. The dune:antidune transition in fine gravel with especial consideration of downstream migrating antidunes. Sedimentology 49, 1269–1282.
Carling, P.A., Burr, D.M., Johnsen, T.F., Brennand, T.A., 2009a. A review of open-channel megaflood depositional landforms on Earth and Mars. In: Burr, D.M., Carling, P.A., Baker, V.R. (Eds.), Megaflooding on Earth and Mars. Cambridge University Press, Cambridge, pp. 33–45.
Carling, P.A., Williams, J.J., Croudace, I., Amos, C.L., 2009b. Formation of mudridge and runnels in the intertidal zone of the Severn Estuary, UK. Cont. Shelf Res., 1913–1926.
Carr, M.J., 1979. Formation of martian flood features by release of water from confined aquifers. J. Geophys. Res. 84, 2995–3007.
Christensen, P.R. et al., 2003. Morphology and composition of the surface of Mars: Mars Odyssey THEMIS results. Science 300, 2056–2061.
Gourronc, M. et al., 2014. One million cubic kilometers of fossil ice in Valles Marineris: Relicts of a 3.5 Gy old glacial land system along the martian equator. Geomorphology 204, 235–255.
Grosswald, M.G., 1999. Cataclysmic Megafloods in Eurasia and the Polar Ice Sheets. Moscow Scientific World, Moscow (in Russian).
Gulick, V.C., Tyler, D., McKay, C.P., Haberle, R.M., 1997. Episodic ocean-induced $CO_2$ greenhouse on Mars: Implications for fluvial valley formation. Icarus 130, 68–86.
Hartmann, W.K., Neukum, G., 2001. Cratering chronology and the evolution of Mars. Space Sci. Rev. 96, 165–194.
Head, J.W. et al., 2005. Tropical to mid-latitude snow and ice accumulation, flow and glaciation on Mars. Nature 434, 346–350.
Hoffman, N., 2000. White Mars: A new model for Mars' surface and atmosphere based on $CO_2$. Icarus 146, 326–342.
Hopper, J.P., Leverington, D.W., 2014. Formation of Hrad Vallis (Mars) by low viscosity lava flows. Geomorphology 207, 96–113.
Ivanov, B.A., 2001. Mars/Moon cratering ratio estimates. Space Sci. Rev. 96, 87–104.
Johnsen, T.F., Brennand, T.A., 2004. Late-glacial lakes in the Thompson Basin, British Columbia: Paleogeography and evolution. Can. J. Earth Sci. 41, 1367–1383.
Kneissl, T., Van Gasselt, S., Neukum, G., 2011. Map-projection-independent crater size–frequency determination in GIS environments – New software tool for ArcGIS. Planet. Space Sci. 59, 1243–1254.
Komatsu, G., Arzhannikov, S.G., Gillespie, A.R., Burke, R.M., Miyamoto, H., Baker, V.R., 2009. Quaternary paleolake formation and cataclysmic flooding along the upper Yenisei River. Geomorphology 104, 143–164.
Koster, E.H., 1978. Fluvial sedimentology. Can. Soc. Pet. Geol. Mem. 5, 161–186.
Leverington, D.W., 2011. A volcanic origin for the outflow channels of Mars: Key evidence and major implications. Geomorphology 132, 51–75.
Lewis, A.R., Marchant, D.R., Kowalewski, D.E., Baldwin, S.L., Webb, L.E., 2006. The age and origin of the Labyrinth, western Dry Valleys, Antarctica: Evidence for extensive middle Miocene subglacial floods and freshwater discharge to the Southern Ocean. Geology 34, 513–516.
Lucchitta, B.K., 1982. Ice sculpture in the martian outflow channels. J. Geophys. Res. 87, 9951–9973.
Lucchitta, B.K., 2001. Antarctic ice streams and outflow channels on Mars. Geophys. Res. Lett. 28 (3), 403–406.
Lucchitta, B.K., Isbell, N.K., Howington-Kraus, A., 1994. Topography of Valles Marineris: Implications for erosional and structural history. J. Geophys. Res. 99, 3783–3798.
Meresse, S., Costard, F., Mangold, N., Masson, P., Neukum, G., Team, H.C.-I., 2008. Formation and evolution of the chaotic terrains by subsidence and magmatism: Hydraotes Chaos, Mars. Icarus 194, 487–500.
Michael, G.G., Neukum, G., 2010. Planetary surface dating from crater size–frequency distribution measurements: Partial resurfacing events and statistical age uncertainty. Earth Planet. Sci. Lett. 294, 223–229.
Michael, G.G., Platz, T., Kneissl, T., Schmedemann, N., 2012. Planetary surface dating from crater size–frequency distribution measurements: A quantitative test of spatial randomness. Icarus 218, 169–177.
Montgomery, D.R. et al., 1997. Evidence for Holocene megafloods down the Tsangpo River gorge, southeastern Tibet. Quaternary Res. 62, 201–207.
Nummedal, D., Prior, D.B., 1981. Generation of martian chaos and channels by debris flows. Icarus 45, 77–86.
Pacifici, A., Komatsu, G., Pondrelli, M., 2009. Geological evolution of Ares Vallis on Mars: Formation by multiple events of catastrophic flooding, glacial and periglacial processes. Icarus 202, 60–77.
Platz, T., Michael, G., Tanaka, K.L., Skinner, J.A., Fortezzo, C.M., 2013. Crater-based dating of geological units on Mars: Methods and application for the new global map. Icarus 225, 806–827.
Rice, J.W., 2000. Flooding and ponding on Mars: Field observations and insights from the polar realms of the Earth. In: Lunar Planet. Sci. XXXI. Abstract #2067.
Rice, J.W., Russell, A.J., Knudsen, O., 2002. Paleohydraulic interpretation of the Modrudalur transverse ribs: Comparisons with martian outflow channels. In: Snorasson, A., Finnsdottir, H.P., Moss, M. (Eds.), The Extreme of the Extremes: Extraordinary Floods. International Association of Hydrological Sciences Red Book.
Rodriguez, J.A.P. et al., 2005. Outflow channel sources, reactivation, and chaos formation, Xanthe Terra, Mars. Icarus 175 (1), 36–57.
Rodriguez, J.A.P., Tanaka, K.L., Miyamoto, H., Sasaki, S., 2006. Nature and characteristics of the flows that carved the Simud and Tiu outflow channels, Mars. Geophys. Res. Lett. 33. http://dx.doi.org/10.1029/2005GL024320, 08S04.
Rotto, S., Tanaka, K.L., 1995. Geologic/geomorphic map of the Chryse Planitia Region of Mars. U.S. Geol. Surv. Misc. Inv. Ser. Map, I-2441-A (1:5000,000).
Schonfeld, E., 1976. On the origin of the martian channels. Eos Trans. American Geophysical Union 57. Abstract 948.
Skinner, J.A., Tanaka, K.L., Platz, T., 2012. Widespread loess-like deposit in the martian northern lowlands identifies Middle Amazonian climate change. Geology. http://dx.doi.org/10.1130/G33513.1.
Teller, J.T., 2004. Controls, history, outbursts, and impact of large late-Quaternary proglacial lakes in North America. In: Gilespie, A., Porter, S., Atwater, B. (Eds.), The Quaternary Period in the United States, INQUA Anniversary Volume. Elsevier, pp. 45–46.
Warner, N.H., Gupta, S., Kim, J.R., Lin, S.Y., Muller, J.P., 2013a. Retreat of a giant cataract in a long-lived (3.7–2.6 Ga) martian outflow channel. Geology 38, 791–794.
Warner, N.H., Sowe, M., Gupta, S., Dumke, A., Goddard, K., 2013b. Fill and spill of giant lakes in the eastern Valles Marineris region of Mars. Geology, 675–678.
Williams, R.M.E., Malin, M.C., 2004. Evidence for late stage fluvial activity in Kasei Valles, Mars. J. Geophys. Res. 109 (E06001). http://dx.doi.org/10.1029/2003JE002178.
Wilson, L., Ghatan, G.J., Head, J.W., Mitchell, K.L., 2004. Mars outflow channels: A reappraisal of the estimation of water flow velocities from water depths, regional slopes and channel floor properties. J. Geophys. Res. 109 (E9).